

Model for wormlike polymers confined between hard walls

J. Z. Y. CHEN¹, D. E. SULLIVAN² and X. YUAN¹

¹ *Department of Physics, University of Waterloo - Waterloo, Ontario, Canada N2L 3G1*

² *Department of Physics, University of Guelph - Guelph, Ontario, Canada N1G 2W1*

received 13 January 2005; accepted in final form 4 August 2005

published online 31 August 2005

PACS. 61.41.+e – Polymers, elastomers, and plastics.

PACS. 64.70.Md – Transitions in liquid crystals.

PACS. 68.47.Mn – Polymer surfaces.

Abstract. – We analyze the structure and phase behavior of long wormlike polymers sterically confined between two parallel, structureless walls, separated by a distance W . We focus on the case where W is comparable to the persistence length ℓ_p of the polymers, $W \sim \ell_p \ll L$, where L is the total contour length of a polymer. We find that three distinct phases (uniaxial, biaxial and condensed) may exist, depending on the polymer density and W , for wormlike chains interacting with each other through the excluded-volume interaction.

The model of wormlike polymers [1, 2] has been widely used to provide fundamental understanding of the structures and dynamics of a large variety of synthetic and biological polymers. A wormlike chain is commonly characterized by its total contour length L and persistence length, ℓ_p , which is related to the local bending energy of segments. For a free, long wormlike polymer ($L \gg \ell_p$), the essential conformational and dynamical properties are similar to those found in the Gaussian model [1–3], which is commonly used for describing flexible polymers, as long as $2\ell_p$ is identified as the effective Kuhn length a [2]. For a single flexible polymer confined between two walls separated by a distance W (*i.e.*, in a slit geometry), the structural information can be well represented by an elegant analytic solution [1]. This solution is valid only in the parameter regime $\ell_p \ll W \ll R_0$, where R_0 is the unperturbed dimension of the polymer, $R_0 \equiv \sqrt{La}$. However, some confined biological molecules function in a different parameter regime where ℓ_p is comparable to the confinement dimension. For example, in a cavity of dimension that is much smaller than the persistence length of a double-stranded DNA molecule (dsDNA), viruses such as the herpesviruses and adenoviruses actively package dsDNA into preformed precursor capsids [4].

This paper serves two purposes. First, we show that, for a confined wormlike polymer without excluded-volume interaction between the segments, where $W \sim \ell_p \ll R_0$, the consideration of local persistency yields structural features that are very different from the above-mentioned analytic solution; in particular, the free energy of the system follows a different dependence on W . Secondly, we consider the fact that closely packed wormlike chains also interact with each other through an orientational-dependent excluded-volume interaction [5]. This interaction is responsible for the formation of liquid-crystal phases that are characterized by orientational ordering of polymer segments [6]. When the excluded-volume interaction is explicitly incorporated in a mean-field treatment, we show that, depending on the monomer density and W , confined wormlike polymers may display three orientational phases, uniaxial,

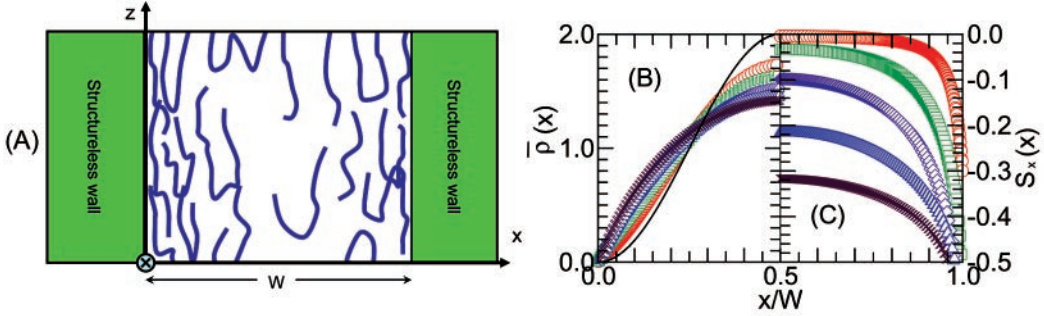


Fig. 1 – (A) Schematic diagram of wormlike chains between two parallel walls and the coordinate system used, (B) left half of the normalized segment density profile, and (C) right half of the orientational order parameter profile. The solid curve in plot (B) represents the limit of $W \gg a$ and can be obtained analytically. Circles, squares, diamonds, triangles, and crosses represent the profiles computationally obtained for $W/a = 6, 4, 2, 1$ and 0.5 , respectively.

biaxial, and condensed. The existence of these liquid crystal phases is known for systems of confined rigid rods between two parallel walls [7,8], but has not been well characterized for confined wormlike chains.

To start with, we review the statistical treatment of a flexible polymer in an external field $V(\mathbf{r})$, acting on a unit segment. The configuration of the polymer is described by a continuous space curve $\mathbf{r}(t)$, where t is the contour coordinate varying from 0 to L/a . The statistical weight, widely used in developing essential statistical-physics approaches to polymers [1,3,9], is described by

$$P[\mathbf{r}(t)] \propto \exp \left[- \int_0^{\frac{L}{a}} dt \left\{ \frac{3}{2a^2} \left| \frac{d\mathbf{r}(t)}{dt} \right|^2 + \beta V[\mathbf{r}(t)] \right\} \right], \quad (1)$$

where $\beta = 1/k_B T$, k_B is the Boltzmann constant and T the temperature. Based on this weight and for long polymers ($R_0 \gg W \gg a$), one can show that $\psi(\mathbf{r})$, the probability that a long polymer portion has an end located at \mathbf{r} , satisfies [10]

$$-\beta\mu\psi(\mathbf{r}) = \left[\frac{a^2}{6} \nabla^2 - \beta V(\mathbf{r}) \right] \psi(\mathbf{r}). \quad (2)$$

Within the parameter regime $R_0 \gg W \gg a$, one is interested in the ground-state solution for $\psi(\mathbf{r})$ and the corresponding eigenvalue (which can be identified with the reduced free energy per segment $\beta\mu$ [11]). For an infinite square well potential in one dimension, $V(\mathbf{r}) = V_w(x) = 0$ for $0 \leq x \leq W$ and $V_w(x) = \infty$ otherwise, eq. (2) has a simple solution: $\psi(x) = A \sin(\pi x/W)$ and $\beta\mu = (\pi^2/6)(a/W)^2$, where A is a normalization constant [1]. The normalized segment density profile⁽¹⁾ across the potential well, $\bar{\rho}(x)$, can therefore be deduced based on the connection condition [10], $\bar{\rho}(x) = [\psi(x)]^2 = 2 \sin^2(\pi x/W)$. Half of $\bar{\rho}(x)$ is plotted as a solid curve in fig. 1B, which is a universal function of x/W , independent of a . Then, the free energy of the entire polymer, F , can be written as the number of segments, L/a , multiplied by the segmental free energy, μ . This leads to $F \equiv \mu L/a \propto k_B T (La/W^2) \propto k_B T (R_0/W)^2$, fully consistent with the result from a simple scaling argument based on, for example, the “blob”

⁽¹⁾Here we use “segment” to refer to a polymer segment that has a contour length equivalent to a , which can be directly related to a monomer length in flexible chains.

picture [3]. The $(R_0/W)^2$ term comes from the loss of entropy by compressing the polymer from a natural dimension R_0 to a small gap of dimension W [3], which is a valid physical picture for the parameter space $a \ll W \ll R_0$.

Can the scaling relation $F/k_B T \sim La/W^2$ (for $a \ll W$) be extended to the regime $W \sim a$ as well? The characteristic physical features at a length scale smaller than a have been ignored in eq. (1). To examine this, we consider the approach taken by Saito, Takahashi, and Yunoki for treating wormlike chains [12], where physical features at length scales smaller than ℓ_p are retained. The configuration of a polymer is again described by a continuous space curve, but the statistical weight depends on the local curvature variation⁽²⁾

$$P \propto \exp \left[- \int_0^{\frac{L}{a}} dt \left\{ \frac{1}{4} \left| \frac{d\mathbf{u}(t)}{dt} \right|^2 + \beta V[\mathbf{r}(t), \mathbf{u}(t)] \right\} \right], \quad (3)$$

where $\mathbf{u}(t)$ is the unit vector $\mathbf{u} \equiv (1/a)d\mathbf{r}(t)/dt$ and $V(\mathbf{r}, \mathbf{u})$ is the external potential acting on a unit segment, a function of both \mathbf{r} and \mathbf{u} . Because orientation is explicitly considered, one introduces the conditional probability that a polymer portion has an end located at \mathbf{r} and pointing in the direction \mathbf{u} , $\Psi(\mathbf{r}, \mathbf{u})$. For $a \ll R_0$ (long polymer), we need to solve [9]

$$-\beta\mu\Psi(\mathbf{r}, \mathbf{u}) = [\nabla_{\mathbf{u}}^2 - a\mathbf{u} \cdot \nabla_{\mathbf{r}} - \beta V(\mathbf{r}, \mathbf{u})]\Psi(\mathbf{r}, \mathbf{u}). \quad (4)$$

Again, we are only concerned with the ground-state solution. The segment density $\rho(\mathbf{r}, \mathbf{u})$ can be readily written in terms of $\Psi(\mathbf{r}, \mathbf{u})$,

$$\rho(\mathbf{r}, \mathbf{u}) = \Psi(\mathbf{r}, -\mathbf{u})\Psi(\mathbf{r}, \mathbf{u}). \quad (5)$$

Note that the two polymer portions, that are connected to form a non-terminal monomer pointing along \mathbf{u} , should have terminal segments pointing along \mathbf{u} and $-\mathbf{u}$, respectively, reflected in the above equation by the two \mathbf{u} variables on the right-hand side. This formalism has been used for studying interfacial properties between two immiscible wormlike polymers [13] and between the isotropic and nematic states of wormlike liquid-crystal polymers [14, 15].

This more general approach is expected to be valid for any ratio of W/a . For the square-well problem, it recovers eq. (2) in the limit of $W/a \gg 1$. Within this limit, the only relevant orientational variable is $\cos\theta_x \equiv \mathbf{u} \cdot \hat{\mathbf{x}}$, where $\hat{\mathbf{x}}$ is a unit vector along the x -axis [13]. Expanding $\Psi(x, \mathbf{u})$ in terms of Legendre functions $P_l(\cos\theta_x)$, $\Psi(x, \mathbf{u}) = \sum_0^\infty \psi_l(x)P_l(\cos\theta_x)$, and substituting this expression into eq. (4) allow us to identify the coupled differential equations that $\psi_l(x)$ must satisfy. One can then show that the l -th order term in the above expansion has the magnitude $(a/W)^l$, and $\psi_0(x)$ satisfies eq. (2) when $W/a \gg 1$. Hence, eq. (2) is a special, asymptotic case of eq. (4).

We now return to the general case of $W \sim a \ll R_0$, which requires numerical consideration of eq. (4) [15]. Caution must be made to impose the proper boundary conditions at the walls. For the geometry of hard walls described in fig. 1, it is clear that the external potential $V_w(x, \mathbf{u}) = \infty$ for $x < 0$ or $x > W$, which is a condition that would be normally invoked in a typical potential-well problem. The situation at $x = 0^+$, however, is more complex; a polymer terminal segment that points to the negative x -direction is not directly influenced by the hard-wall steric interaction, hence has a non-zero density distribution; on the other hand, a polymer terminal segment that points to the positive x -direction is subject to the hard-wall steric interaction [16]. This implies that $V_w(0^+, \mathbf{u}) = \infty$ for $\mathbf{u} \cdot \hat{\mathbf{x}} > 0$ and $V_w(0^+, \mathbf{u}) =$

⁽²⁾Hereafter we use a explicitly ($a = 2\ell_p$) in order to make a direct comparison with the properties based on eq. (1).

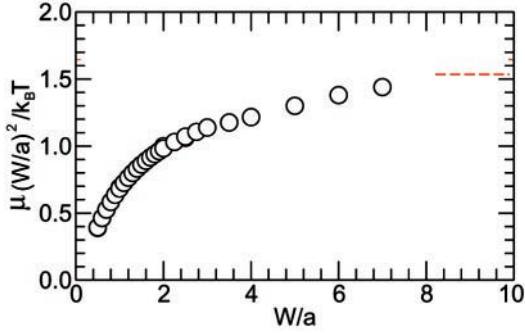


Fig. 2

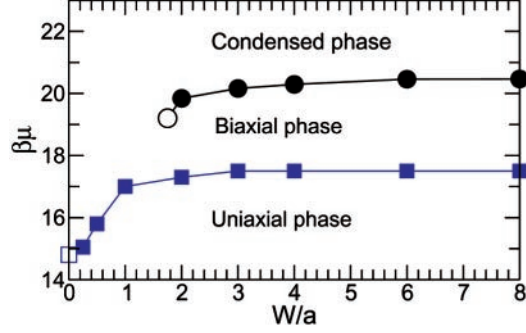


Fig. 3

Fig. 2 – Numerical solution for the reduced segmental chemical potential, $\mu(W/a)^2/k_B T$, as a function of the ratio between slit width W and Kuhn length a for a wormlike chain. The dashed line represents the asymptotic limit $\pi^2/6$, based on the model for flexible chains.

Fig. 3 – Phase diagram for wormlike chains confined between walls of width W , in terms of the reduced chemical potential $\beta\mu$ per effective Kuhn segment. Filled symbols represent the numerical solution to eqs. (4)-(7) based on which solid curves (first-order phase boundaries) are projected. Open symbols represent the critical points.

0 for $\mathbf{u} \cdot \hat{\mathbf{x}} < 0$; according to the same rational, $V_w(W - 0^+, \mathbf{u}) = \infty$ for $\mathbf{u} \cdot \hat{\mathbf{x}} < 0$ and $V_w(W - 0^+, \mathbf{u}) = 0$ for $\mathbf{u} \cdot \hat{\mathbf{x}} > 0$.

Using these boundary conditions and implementing Legendre expansions for the angular dependence in both $\Psi(x, \mathbf{u})$ and $V_w(x, \mathbf{u})$, we have numerically solved the eigenproblem in eq. (4) for any value of W/a . Figure 2 shows the numerical solution for the eigenvalue $\beta\mu$ as a function of W/a . Note that $\beta\mu$ approaches the asymptotic behavior $(\pi^2/6)(a/W)^2$ at $W/a \gg 1$, in agreement with the analytic solution to eq. (2). The crossover to a linear $\beta\mu \propto a/W$ dependence is also visible in the figure, as W/a goes to 0. Correspondingly, the free energy of the chain displays a crossover from $F/k_B T = La/W^2$ (for $a \ll W$) to L/W (for $W \ll a$) as W/a varies. In addition, we have plotted the normalized segment density, $\bar{\rho}(x) = \int d\mathbf{u} \rho(x, \mathbf{u}) / \int dx d\mathbf{u} \rho(x, \mathbf{u})$, and the order parameter, $S_x(x) \equiv \langle P_2(u_x) \rangle$ in fig. 1B and C for several values of W/a , where $\langle \dots \rangle$ is performed in reference to the conditional density probability function in eq. (5) with a fixed x . The illustration shows that as W/a is decreased from a rather large value (circles where $W/a = 6$) to a small value (crosses where $W/a = 0.5$), $\bar{\rho}(x)$ deviates from the universal function predicted from eq. (2) (solid curve); instead of occupying the central region between the walls to maximize the entropy, the polymer segments are forced towards the near-wall regions by small W . In the meantime, polymer segments near the walls develop significant orientational ordering, lying parallel to the walls — a value $-1/2$ for S_x would imply that the segments are perfectly parallel to the surface of the wall.

So far we have discussed the structure of wormlike chains without mutual segment-segment interactions. To include excluded-volume interactions, a wormlike chain can be treated as a cylindrical filament (which can still be described by a space curve specifying the filament axis) characterized by a cross-sectional diameter D . Onsager derived a free energy expression based on the second-virial coefficient approximation for the excluded-volume interaction between two rods of an arbitrary relative orientation [5]. The Onsager approximation is considered accurate for long polymers [6], where $L \gg a \gg D$, a condition that can be easily satisfied by most polymer systems, in particular, DNA molecules. To describe the current system, the

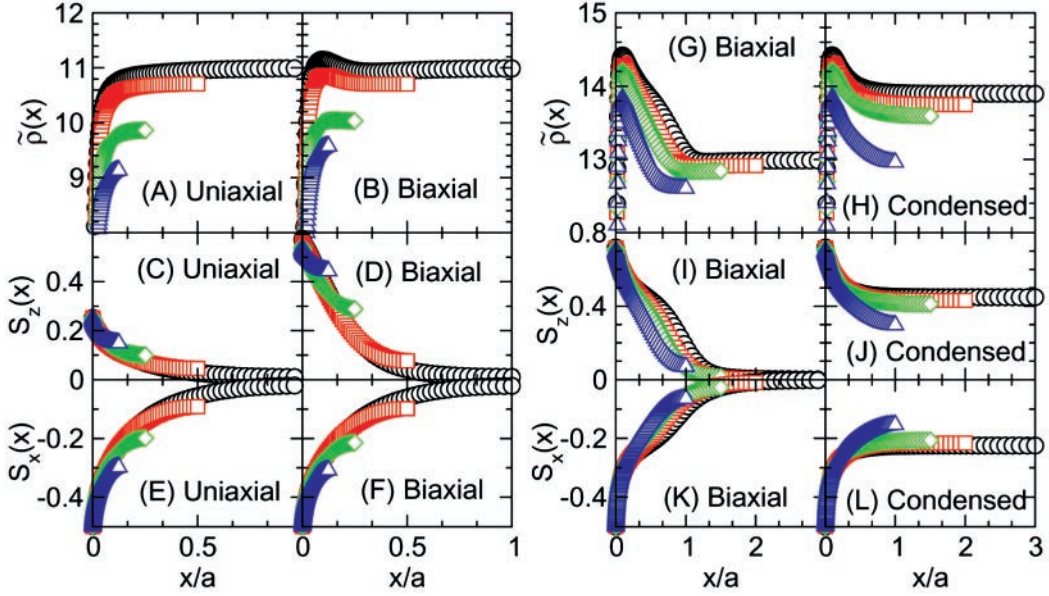


Fig. 4 – Density and order parameter profiles between $0 \leq x/a \leq \frac{1}{2}W/a$. For the biaxial and uniaxial states (A)-(F), we have plotted the curves for $W/a = 2$ (circles), 1 (squares), 0.5 (diamonds), and 0.25 (triangles) at the uniaxial-biaxial transition, corresponding to $\beta\mu = 17.3, 17.0, 16.0$ and 15.5, respectively. For the condensed and biaxial states (G)-(L), we have plotted the curves for $W/a = 6$ (circles), 4 (squares), 3 (diamonds), and 2 (triangles) at the biaxial-condensed transition, corresponding to $\beta\mu = 20.4, 20.3, 20.2$ and 19.9, respectively.

interaction between a polymer segment and others is approximated by a mean-field background potential energy $U(x, \mathbf{u})$ acting on this segment. Within the Onsager approximation, this is given by [6, 15],

$$\beta U(x, \mathbf{u}) = 2a^2 D \int d\mathbf{u}' \rho(x, \mathbf{u}') |\mathbf{u} \times \mathbf{u}'|. \quad (6)$$

The potential $V(x, \mathbf{u})$ in eq. (4) now reads

$$V(x, \mathbf{u}) = U(x, \mathbf{u}) + V_w(x, \mathbf{u}). \quad (7)$$

Equations (4)-(7) completely specify a set of self-consistent equations which we have solved numerically by implementing a spherical-harmonic expansion⁽³⁾ for the angular dependence of all involved functions [15]. We have found that three distinct structures are possible, depending on the magnitude of W/a and $\beta\mu$ (see fig. 3); in reduced units, the reduced segment density $\bar{\rho}(x) \equiv a^2 D \int d\mathbf{u} \rho(x, \mathbf{u})$ is fully controlled by these two parameter.

Consider a system where $W/a > 1.75$ (fig. 3). At low $\beta\mu$ (hence low segment density), the excluded-volume interaction between segments is less important and the orientational ordering of those near-wall segments is mainly the consequence of the steric interaction with the wall. Within a distance of a from the wall, there exists a depletion layer of polymer segments, as $\bar{\rho}(x)$ in fig. 4A shows. At $x = 0^+$, $S_x(x)$ attains the value $S_x(0^+) = -1/2$, while both $S_y(x) = \langle P_2(\mathbf{u} \cdot \hat{\mathbf{y}}) \rangle$ and $S_z(x) = \langle P_2(\mathbf{u} \cdot \hat{\mathbf{z}}) \rangle$ have the value $\frac{1}{4}$, where $\hat{\mathbf{y}}$ and $\hat{\mathbf{z}}$

⁽³⁾In these expansions, terms up to $l = 12$ have been considered, which is adequate for describing the orientational ordering in this type of systems [15].

are the unit vectors along the y and z axes. Only two of these three order parameters are independent ($S_x(x) + S_y(x) + S_z(x) = 0$). Throughout the entire region, the *uniaxial* symmetry $S_z(x) = -S_x(x)/2$ is maintained (figs. 4C and E).

At a fixed W/a , increasing $\tilde{\rho}$ corresponds to increasing $\beta\mu$. As $\beta\mu$ approaches 17.6 (more exactly, the solid curve associated with squares in fig. 3), a first-order phase transition to a biaxial phase, that has different orientational properties, can be seen. Khokhlov and Semenov were the first to suggest that a nematic liquid-crystal phase can form provided that $\tilde{\rho}$ is high enough, where the orientation-dependent Onsager interaction is the mechanism responsible for this transition [6]. We see here the manifestation of a similar principle at work in a confined system. Polymer segments far from the wall are still oriented nearly randomly and give rise to the similar density as in a uniaxial phase. The segments close the wall begin to develop a density-enhanced layer with nematic characteristics (fig. 4B); a preferred direction parallel to the wall surface is selected as the local nematic direction (defined as z in fig. 1). Orientational order parameters in this phase display typical biaxiality: $S_z(x) > |S_x(x)|/2$ (fig. 4D and F).

As the overall density is further increased, the biaxial phase remains stable as long as the density far from the wall is below the value in the isotropic phase of the bulk isotropic-nematic (IN) transition, $\tilde{\rho}_I = 13.048$ (corresponding to $\beta\mu_{IN} = 20.50$) [6, 17]. The density-enhanced layer near the wall develops stronger nematic characteristics and the local density may even exceed $\tilde{\rho}_N = 14.039$, the value in the nematic phase of the bulk IN transition (see fig. 4G). The surface layer expands beyond a and develops into a thick partial wetting layer, so long as the system width is allowed to maintain such a surface layer. For very large W/a , this behavior of the biaxial phase continues until $\beta\mu$ reaches $\beta\mu_{IN}$, where the thickness of the wetting layer diverges, which results in complete wetting by the nematic phase at a single wall [16]. For smaller W/a , however, the dense wetting layers extending from both walls tend to merge, resulting in a new (capillary) *condensed* phase (see fig. 4H), which becomes stable after $\beta\mu$ reaches the biaxial-condensed phase boundary in fig. 3. After this phase transition, the density within the entire space between the walls jumps to a value comparable to $\tilde{\rho}_N$. As demonstrated by fig. 4J and L, the orientational order parameters still display typical biaxiality: $S_z(x) > |S_x(x)|/2$, but the average order parameter S_z grows and approximately reaches the asymptotic value $S_z = 0.4618$, found for the bulk isotropic-nematic transition [6, 17]. Ultimately, as $W/a \rightarrow \infty$, the first-order biaxial-condensed transition becomes a second-order complete wetting transition discussed in ref. [16].

This scenario of three stable phases for a fixed W/a needs to be revised for $W/a < 1.75$. Because the space between the walls is so narrow, the system does not support the adequate development of the partial wetting biaxial state; the latter might already have a wetting width that exceeds W . The transition between the partial wetting and condensed states is now continuous without any signature of a phase transition (fig. 3). The first-order phase boundary between the biaxial and condensed phases terminates at a critical point near $W/a = 1.7 \pm 0.1$ and $\beta\mu = 19.2 \pm 0.3$.

Qualitatively, long wormlike chains can be viewed as rods of length $2\ell_p$ freely jointed together; the three phases found here can be compared to similar phases that appear in the system of rodlike molecules between walls [7, 8]. There is, however, an important difference between our phase diagram and that in ref. [7]. In fig. 3, the uniaxial-biaxial transition is a first-order line ending at a second-order point at $W/a = 0$ (a quasi-two-dimensional system [18]). This can be further augmented by a general symmetry analysis of liquid-crystal orientations, independent of the underlying molecular structures (polymers or hard rods) [19]. In contrast, ref. [7] suggested that the uniaxial-biaxial transition is second order based on a numerical analysis of the Zwanzig model [20].

In summary, we have demonstrated that the conventionally used flexible-chain model

(eq. (1)) is inadequate for describing wormlike chains confined between two walls, even in the limit of $L \gg \ell_p$. With the inclusion of the excluded-volume interaction, we have also shown that three distinct phases, uniaxial, biaxial, and condensed, may exist in wormlike polymers confined between two parallel walls.

* * *

We thank NSERC for financial support and SHARCNET for computation time.

REFERENCES

- [1] DOI M. and EDWARDS S. F., *The Theory of Polymer Dynamics* (Oxford University Press, New York) 1986.
- [2] YAMAKAWA H., *Modern Theory of Polymer Solutions* (Harper and Row, New York) 1971.
- [3] DE GENNES P.-G., *Scaling Concepts in Polymer Physics* (Cornell University Press, Ithaca) 1979.
- [4] See, example, RIXON F. J., *Semin. Virol.*, **4** (1993) 135; D'HALLUIN J.-C. *et al.*, *J. Virol.*, **26** (1978) 357; EARNSHAW W. C. and HARRISON C. S., *Nature*, **268** (1977) 598; KINDT J. *et al.*, *Proc. Natl. Acad. Sci. (U.S.A.)*, **98** (2001) 13671; EVILEVITCH A. *et al.*, *Proc. Natl. Acad. Sci. (U.S.A.)*, **100** (2003) 9292; TZLIL S. *et al.*, *Biophys. J.*, **84** (2003) 1616; HUD N. V., *Biophys. J.*, **69** (1995) .
- [5] ONSAGER L., *Ann. N.Y. Acad. Sci.*, **51** (1949) 627.
- [6] KHOKHLOV A. R. and SEMENOV A. N., *Physica A*, **112** (1982) 605.
- [7] VAN ROIJ R., DIJKSTRA M. and EVANS R., *Europhys. Lett.*, **49** (2000) 350; *J. Chem. Phys.*, **113** (2000) 7689.
- [8] DIJKSTRA M., VAN ROIJ R. and EVANS R., *Phys. Rev. E*, **63** (2003) 051703; CHRZANOWSKA A., TEIXEIRA P. I. C., EHRENTAUT H. and CLEAVER D. J., *J. Phys. Condens. Matter*, **13** (2001) 4715; RODRIGUEZ-PONCE I., ROMERO-ENRIQUE J. M. and RULL L. F., *J. Chem. Phys.*, **122** (2005) 014903; DE LAS HERAS D., VELASCO E. and MEDEROS L., *J. Chem. Phys.*, **120** (2002) 4949; HARNAU L. and DIETRICH S., *Phys. Rev. E*, **66** (2002) 051702; LAGOMARSINO M. C., DOGTEROM M. and DIJKSTRA M., *J. Chem. Phys.*, **119** (2003) 3535. CHRZANOWSKA A., *J. Comp. Phys.*, **191** (2003) 265.
- [9] FREED K. F., *Adv. Chem. Phys.*, **22** (1972) 1.
- [10] HELFAND E., *J. Chem. Phys.*, **62** (1975) 999.
- [11] GROSBERG A. YU. and KHOKHLOV A. R., *Statistical Physics of Macromolecules* (American Institute of Physics, New York) 1994.
- [12] SAITO N., TAKAHASHI K. and YUNOKI Y., *J. Phys. Soc. Jpn.*, **22** (1967) 219.
- [13] MORSE D. C. and FREDRICKSON G. H., *Phys. Rev. Lett.*, **73** (1994) 3235; SCHMID F. and MÜLLER M., *Macromolecules*, **28** (1995) 8639.
- [14] GROSBERG A. YU and PACHMOV D. V., *Liq. Cryst.*, **10** (1991) 539.
- [15] CUI S.-M., AKCAKIR O. and CHEN Z. Y., *Phys. Rev. E*, **51** (1995) 4548.
- [16] CHEN Z. Y. and CUI S.-M., *Phys. Rev. E*, **52** (1995) 3876.
- [17] ODIJK T., *Macromolecules*, **19** (1986) 2313; VROEGE G. J. and ODIJK T., *Macromolecules*, **21** (1988) 2848; CHEN Z. Y., *Macromolecules*, **26** (1993) 3419.
- [18] CHEN Z. Y., *Phys. Rev. Lett.*, **71** (1993) 93.
- [19] CHEN J. Z. Y., SULLIVAN D. E. and YUAN X., unpublished.
- [20] ZWANZIG R., *J. Chem. Phys.*, **39** (1963) 1714.